LANGMUIR

pubs.acs.org/Langmuir Article

# Unlocking the Potential of Liquid Plasma Polymer Films: Characterizing Aging Effects and Their Impact on the Wrinkling Phenomenon

Suyog A. Raut, Nathan Vinx, David Tromont, Philippe Leclère, Damien Cossement, Rony Snyders, and Damien Thiry*

Cite This: https://doi.org/10.1021/acs.langmuir.4c01552 Read Online

ACCESS | Metrics & More | Article Recommendations

**ABSTRACT:** Here, we present the study of the intricate dynamics between the physicochemical properties of liquid propanethiol plasma polymer films (PPFs) and the formation of wrinkles in PPF/Al bilayers. The study investigates the effect of liquid PPF aging in the air before top Al layer deposition by magnetron sputtering on the wrinkling phenomenon for 4 days. Thanks to atomic force microscopy, the wrinkle dimensions were found to decrease by approximately 55% in amplitude and 66% in wavelength, correlated with an increase in the viscosity of the PPF over the aging duration (i.e., from less than $10^7$ to $10^{10}$ Pa·s). This behavior is not linked to alterations in cross-linking degree as evidenced by time-of-flight secondary ion mass spectrometry experiments but rather to network densification driven by the inherent molecular chain mobility due to the viscous state of the PPF. X-ray photoelectron spectroscopy measurements emphasizing the absence of oxidation of the PPF over the aging duration support this, revealing a unique aging mechanism distinct from other plasma polymer families. Overall, this study offers valuable insights into the design and application of mechanically responsive PPFs involved in bilayer systems, paving the way for advancements in nanotechnology and related fields.

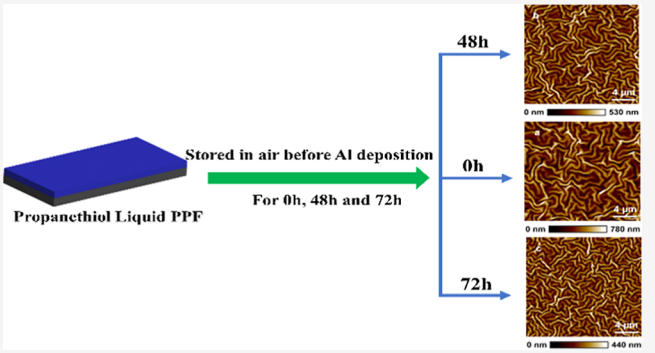


## 1. INTRODUCTION

Over the past several years, plasma technologies have garnered increasing attention due to their capacity to enhance the surface properties of raw materials by either activating the surface or depositing new, valuable layers.[1] Among the plethora of plasma techniques available, plasma polymerization, a process belonging to the plasma-enhanced chemical vapor deposition category, stands out as a particularly compelling method for creating organic thin films known as plasma polymer films (PPFs).[2] The process is based on the activation in a plasma of organic vapor, resulting in the formation of reactive species, including radicals and, to a lesser extent, ions. A PPF is then formed due to the condensation of the reactive species on surfaces exposed to the plasma. The unique growth mechanism, driven by numerous and intricate gas-phase and surface reactions, is responsible for the exceptional properties of PPFs, including their thermal stability, strong adhesion to various substrates, and wide range of chemical compositions as well as their uniqueness, such as the absence of repeating units in their polymeric network.[3,4] Moreover, the simplicity, low environmental impact, and cost-effectiveness position the plasma polymerization process as a reliable technique for producing thin films with vast potential applications, including the biomedical field,[5,6] corrosion protection,[7,8] electronics,[9,10] and more.

In recent decades, there has been a significant focus on fine-tuning the chemical composition of PPFs, which is of interest for biological applications. Substantial advancements have been achieved, particularly in nitrogen-,[11] oxygen-,[12] chlorine-,[13] and sulfur[14]-based PPFs.[15−19] While the mechanical properties of PPFs were previously overlooked, they were generally regarded as rigid and elastic materials, and recent literature has highlighted their significance. Indeed, beyond focusing on the chemical composition, the precise control of these mechanical properties has become a critical requirement for advancing the applications of PPFs, particularly for modulating the biological response of the material.[20]

Received: April 25, 2024
Revised: June 3, 2024
Accepted: June 21, 2024

Our research group has recently achieved a breakthrough in tailoring the mechanical properties of propanethiol-based PPFs by carefully controlling the substrate temperature ($T_s$) during deposition.[21] We observed a remarkable transition from a highly viscous liquid to a rigid elastic solid as $T_s$ increased within a narrow temperature range, specifically from 10 to 45 °C. Leveraging the newfound capability to create mechanically responsive PPFs, we have developed various strategies for producing nanostructured thin films, focusing on implementing bilayer systems of interest for fabricating flexible electrodes.[14] For instance, we have shown that a bilayer system composed of a liquid PPF as the bottom layer and an aluminum coating deposited via magnetron sputtering as the top thin film exhibits a spontaneous surface reorganization phenomenon characterized by the appearance of wrinkles.[10] Our results have indicated that the dimensions of these wrinkles can be tuned in a wide range by modulating the thickness of the PPF bottom layer.[22,23] Notably, the wrinkled bilayers obtained in our experiments were created by consecutively depositing the aluminum layer directly after synthesizing the thin film on the PPF bottom. The influence of the time between the two steps of this process was primarily overlooked.

Moreover, it is well-known in plasma polymerization that PPFs undergo an aging effect involving various physicochemical reactions, including oxidation when exposed to ambient air and surface reorganization of the polymeric network.[18,24,25] On this basis, the potential influence of aging time, spanning the duration between PPF synthesis and aluminum deposition, on the wrinkling phenomenon represents an intriguing aspect that requires thorough investigation.

Within this context, the primary objective of this study is to comprehensively examine the aging phenomenon observed in liquid propanethiol PPFs and its impact on the morphological reorganization process when involved as a compliant material in PPF/Al bilayer systems. We aim to shed light on the underlying mechanisms responsible for this aging effect. To achieve this, we will conduct a multifaceted analysis. First, we will assess the mechanical properties of PPFs over time using atomic force microscopy (AFM). This will provide valuable insights into how these properties change as PPF ages. Additionally, to gain a deeper understanding of the key factors driving the evolution of PPF's mechanical properties, we will scrutinize the chemical composition and cross-linking degree of the PPF. This will be accomplished through X-ray photoelectron spectroscopy (XPS) and time-of-flight secondary ion mass spectrometry (ToF-SIMS).

## 2. EXPERIMENTAL SECTION

**2.1. Substrate Preparation.** PPFs based on propanethiol were deposited onto 1 × 1 $cm^2$ silicon wafers using 1-propanethiol (99%, Sigma-Aldrich). The substrates were meticulously cleaned with 1-isopropanol through three cycles and then dried under a nitrogen flow before being introduced into the deposition chamber.

**2.2. Plasma Polymerization.** Depositions were conducted within a stainless-steel vacuum chamber measuring 65 cm long and 35 cm in diameter. The reactor underwent evacuation using a sequence of turbomolecular and primary pumps, achieving a residual pressure below 2 × $10^{-6}$ Torr. Additional specifics about the deposition chamber can be found elsewhere.[26] Throughout the deposition process, plasma was sustained by a water-cooled copper coil (10 cm in diameter) positioned 10 cm from the sample surface inside the chamber. The coil was connected to an RF (13.56 MHz) power supply (Advanced Energy) via a matching network. Depositions were carried out at a constant pressure of 40 mTorr, regulated by a throttle valve connected to a capacitive gauge. The precursor flow rate remained constant at 10 sccm, and the power applied to the coil was set at 40 W for all experiments. The substrate temperature was monitored using a thermocouple attached to the substrate holder to maintain consistent conditions. External control using liquid nitrogen ensured a constant substrate temperature of 10 ± 1 °C, with the temperature stabilized for 30 min before initiating the deposition to establish thermal equilibrium between the substrate holder and the substrate surface. The choice of this experimental condition is guided by our previous work on propanethiol PPFs, which enabled the synthesis of a liquid-based thin film.[21]

**2.3. Aluminum Deposition.** Aluminum top layers, set at a thickness of 50 nm, were deposited onto propanethiol PPFs using magnetron sputtering in a secondary chamber. The deposition process involved an aluminum target measuring 5 cm in diameter within an inert atmosphere. Argon (Ar) was introduced at a fixed flow rate of 40 sccm, and the pressure was maintained at 7 mTorr. A power of 100 W was applied to the target during the sputtering process. A comprehensive account of the experimental setup is available in a detailed description elsewhere.[21] Before the deposition of Al coatings, the PPFs were stored in the air, varying the aging duration from 0 (i.e., as-deposited) to 96 h.

**2.4. Topography Measurements.** The topography of the PPF/Al bilayer system was captured by AFM using a Bruker Multimode 8 microscope working in tapping mode scanning, equipped with a Nanoscope V controller. Silicon tips labeled "RFESPA-190," commercially available from Bruker Nano Inc. (Santa Barbara, CA), were employed. The resonance frequency at which the acquisitions were made was about 190 kHz, and the cantilever stiffness was about 35 N/m. The AFM images were analyzed using the "Nanoscope Analysis" software. The presented images are in their original recorded state, with consideration given to plane fitting processing.

**2.5. Viscosity Measurements.** A two-step AFM procedure was employed to assess the viscosity of propanethiol PPFs. The AFM setup utilized a Bruker Multimode 8 microscope with a Nanoscope V controller to induce surface modification (i.e., scratching of the polymer film) in contact mode. Subsequently, in a second step, the microscope linked to a NANONIS external controller (by Specs) was switched to tapping mode measurements following the film scratching. Silicon tips from BudgetSensors (ElectriMulti75-G) were utilized for scratching, featuring a resonance frequency of approximately 62.77 kHz, a typical radius of curvature below 25 nm, and a cantilever spring constant of 1.4251 N/m, determined on cleaned Silicon. The initial step of the analysis involved a large force of 190 nN of the cantilever onto the PPF surface, executing a scanning along a unidirectional line by turning off the slow axis scan spanning over 6 $\mu$m for 10 min. Subsequently, the resulting perturbation or "scratch" was imaged over time perpendicular to the virtual line direction to enhance measurement precision in tapping mode. The temporal evolution of the scratch profile was then examined, providing insights into the relaxation dynamics of the PPF, directly correlated with the physicochemical properties of the layer and, ultimately, the viscosity of the PPF by using a procedure described in a previous study.[27]

**2.6. Chemical Composition Measurements.** The chemical composition of PPFs was investigated through XPS. Employing a PHI 5000 Versa Probe apparatus directly interfaced with the deposition chamber under vacuum conditions, a monochromatized Al K$\alpha$ line (1486.6 eV) served as the photon source. The atomic relative concentration of each element was determined by calculating peak areas, taking into account the corresponding photoionization cross sections, the electron inelastic mean free path, and the transmission function of the spectrometer.

**2.7. Cross-Linking Degree Evaluation.** Static ToF-SIMS analyses were conducted on PPFs employing a ToF-SIMS IV instrument manufactured by IONTOF GmbH. Spectra were obtained utilizing a 10 keV $Ar^+$ ion beam at a current of 0.75 pA, systematically rastered over a scan area measuring 300 × 300 $\mu m^2$ for 125 s, specifically in positive mode. The principal component analysis (PCA) method analyzed the spectra using the SIMCA-P13 software


https://doi.org/10.1021/acs.langmuir.4c01552
Langmuir XXXX, XXX, XXX−XXX

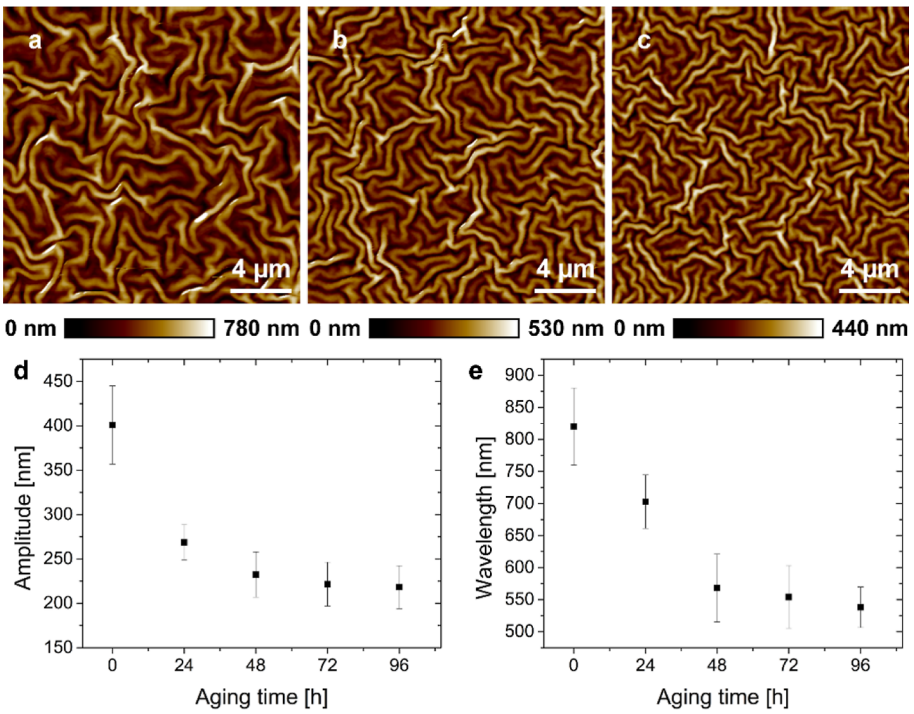


**Figure 1.** 2D AFM images of 285 nm-thick PPF/50 nm-thick Al bilayer for a PFF aging time of (a) 0 h, (b) 48 h, and (c) 72 h. (d,e) represents the evolution of the wrinkles' amplitude and wavelength, respectively, with the PPF aging time.

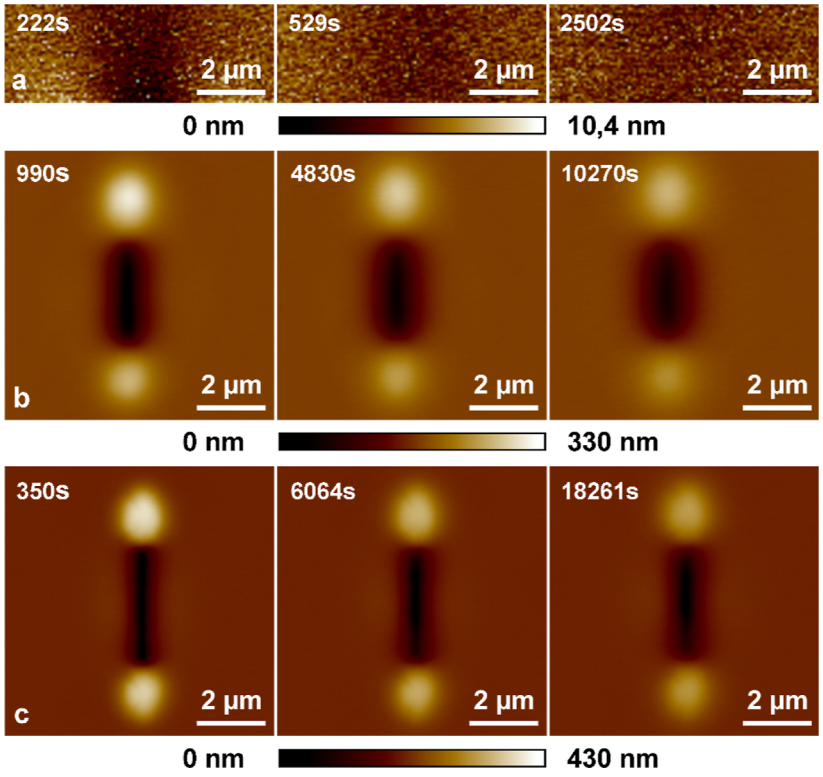


**Figure 2.** AFM images of PPFs (without the Al layer) after scratching for three aging times: (a) as-deposited, (b) after 48 h, and (c) after 96 h.

supplied by Umetrics, Sweden. Before multivariate analysis, each spectrum was normalized to the total ion count number, mean-centered, and scaled. More details about the PCA treatment can be found elsewhere.[28] For reproducibility purposes, eight different locations on the surface of each sample were accounted for ToF-SIMS analyses.

## 3. RESULTS AND DISCUSSION

The stability of the mechanical properties of PPFs was examined over time. It is widely acknowledged that wrinkling phenomena are contingent upon the mechanical characteristics of the bottom and top layers.[29−32] Consequently, as the sole variable parameter, conducting wrinkling experiments on


https://doi.org/10.1021/acs.langmuir.4c01552
Langmuir XXXX, XXX, XXX−XXX

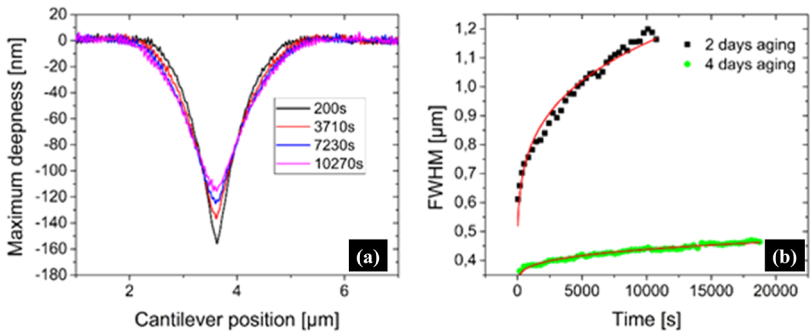


**Figure 3.** (a) Detailed evolution of the scratch profile over time for the PPF aged 48 h, showing changes in the depth and width of the scratch. (b) Graph displaying both the empirical data (dots) and the fitted curves (lines) for the evolution of the fwhm of the scratch profile, comparing the 48 h-aged PPF (black) and the 96 h-aged PPF (red), illustrating the differences in relaxation kinetics between the two aging periods.

comparable PPF samples with varying intervals between the synthesis of the PPF layer and aluminum deposition can provide invaluable insights into the temporal evolution of PPF mechanical behavior. For this purpose, five identical PPF samples were synthesized simultaneously. Subsequently, an aluminum top layer deposition was conducted directly on one of these PPF samples to induce a wrinkled surface. Subsequent aluminum depositions were carried out every 24 h on different PPF samples stored in the air from this batch to generate wrinkling on PPFs with distinct aging times.

Inference from Figure 1 reveals a rapid initial decline followed by a gradual reduction in the dimensions of the wrinkles with increasing PPF aging time. An analysis software is used to obtain a vertical cross-section and measure wrinkles' size. The height difference between the peak and valley is then measured to determine the amplitude of the wrinkles. Additionally, the distance between consecutive peaks and valleys is measured to determine the wavelength dimensions of the wrinkles. Specifically, the amplitude diminishes from 400 ± 44 to 218 ± 24 nm and the wavelength from 820 ± 60 to 537 ± 32 nm over a PPF aging period of 4 days. These findings suggest a discernible evolution in the mechanical properties of the PPF over time.

Specific AFM experiments were conducted to thoroughly investigate the temporal evolution of PPF mechanical behavior. In this regard, the AFM tip was pressed onto the film surface, sweeping along a virtual line spanning 2−5 $\mu$m. This manipulation induced the formation of a scratch of a depression line on the PPF surface, as illustrated in Figure 2. Subsequently, the PPF surface was systematically imaged over time by AFM to study the viscosity of the system's relaxation dynamics, which is correlated to the layer's mechanical properties.[21] Figure 2 represents the AFM images depicting the surface relaxation of PPFs (without the Al layer) for varying aging times (i.e., as deposited, 48 h, and 96 h).

The PPF surface undergoes relaxation, gradually reverting to its initial perturbation shape. At first sight, the relaxation kinetic decreases with the aging time, revealing a variation in the mechanical properties of PPFs during their storage in the air.

The perturbation profile was scrutinized to evaluate the evolution of the viscosity of the PPF with aging time. Figure 3a shows that the hole's depth decreases while the perturbation's width expands over time. Considering a viscous thin film, the relaxation dynamic can be modeled using a two-dimensional Stokes equation in the lubrication regime. Solving the system equations under our experimental conditions leads to eq 1[21]

$$\text{fwhm} \sim \left(\frac{\gamma}{\eta} h_0^{\,3}\right)^{1/4} t^{1/4} \tag{1}$$

where fwhm represents the full width at half-maximum of the perturbation [$\mu$m], $\gamma$ denotes the PPF surface tension [N/m], $\eta$ signifies the viscosity [N·s·m$^{-2}$], $h_0$ denotes the film thickness [nm], and $t$ stands for time [s]. The comprehensive mathematical treatment for solving the system equations can be found elsewhere.[21]

According to eq 1, the scratch width evolves with time dependence following a power law with an exponent value of 1/4. Consequently, the fwhm of the perturbation profiles was assessed over time, as depicted in Figure 3b, solely for 2 day (48 h)- and 4 day (96 h)-aged PPFs; the relaxation dynamic of the as-deposited PPF being too fast for enabling an accurate temporal evolution of the fwhm (see Figure 2a). For both PPFs, eq 1 notably aligns with our experimental data concerning the evolution of the half-width maximum of the scratch, as evidenced by a Pearson correlation coefficient of 0.97 for both cases (Figure 3b). In our experiments, the viscosity of both layers can be evaluated from the fitting data, considering a surface tension value of $10^{-2}$ N/m and a thickness value ($h$) fixed at 2.5 × $10^{-7}$ m. The obtained viscosity values are estimated to be $10^7$ and $10^{10}$ Pa·s for the 2 day (48 h)- and 4 day (96 h)-aged PPFs, respectively. As evidenced by its lower recovery time, it can be concluded that the as-deposited PPF has a viscosity lower than $10^7$ Pa·s.

The evolution in the wrinkles' dimensions of PPF/Al bilayers depicted in Figure 1 can, therefore, be correlated with the evolution of PPF mechanical properties, i.e., an increase in the viscosity over aging time. Das et al. observed that for Al thin films deposited on polydimethylsiloxane, the wrinkle dimensions depended on the viscoelastic properties of the viscous-state polymer in metal/polymer bilayers.[33] They noted a decrease in wrinkle dimensions with an increase in the viscous and elastic components of the polymer.

The evolution in the mechanical properties of PPFs over time may be attributed to an increase in the cross-linking degree, limiting the chain mobility and increasing the material's viscosity.[34] Indeed, it is widely acknowledged in plasma polymerization that trapped radicals exist within the matrix of most PPFs. These radicals are primarily responsible for undesired effects, such as the postsynthesis oxidation of the layer.[18] Furthermore, Vasilev et al. also demonstrated an increase in the cross-linking degree of the PPF with aging time due to the recombination of radicals from adjacent molecular segments, especially for low-cross-linked PPFs.[25] This


https://doi.org/10.1021/acs.langmuir.4c01552
Langmuir XXXX, XXX, XXX−XXX

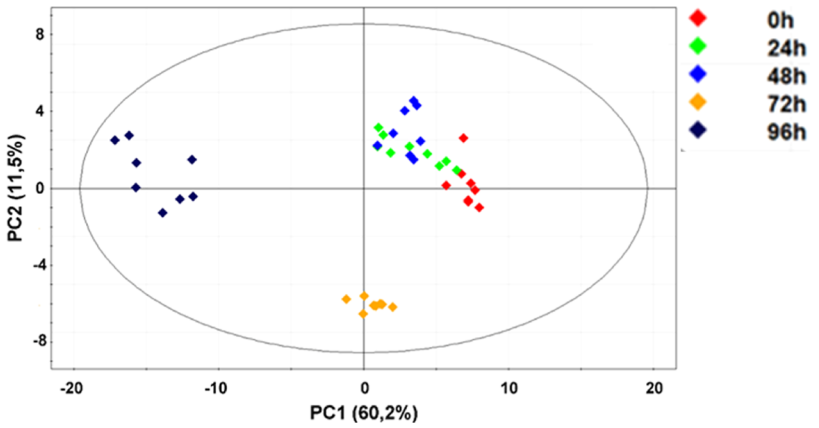


**Figure 4.** Scores plot illustrating the sample discrimination as a result of PCA treatment of the ToF-SIMS data.

**Table 1. Most Influential Loadings Revealed by the PCA of the Positive ToF-SIMS Data and Their Corresponding "Average Fragments" and C/H Ratios**

| PC1 loadings | <0 | >0 |
|---|---|---|
| | $C_4H_7^+$, $C_5H_9^+$, $C_5H_{11}^+$, $C_4H_9^+$, $C_7H_{11}^+$, $C_5H_{10}^+$, $C_6H_{11}^+$, $C_4H_8^+$, $C_7H_{13}^+$, $C_5H_7^+$, $C_6H_{13}^+$, $C_4H_6^+$, $C_5H_8^+$, $C_6H_9^+$, $C_8H_{13}^+$, $C_7H_{12}^+$, $C_9H_{15}^+$, $C_8H_{15}^+$, $C_6H_{10}^+$, $C_3H_6^+$, $C_4H_5^+$, $C_4H_4^+$, $C_2H_5^+$ | $C_5H_5S_2^+$, $CH_3^+$, $C_2H_3^+$, $C_6H_9S^+$, $C_5H_5S^+$, $CH_3S^+$, $C_4H_5S^+$, $C_5H_7S_2^+$, $C_6H_7S^+$, $C_2H_2^+$, $C_4H_5S_2^+$ |
| average fragment | $C_{5.4}H_{9.4}^+$ | $C_{4.7}H_{6.9}^+$ |
| C/H ratio | 0.57 | 0.68 |

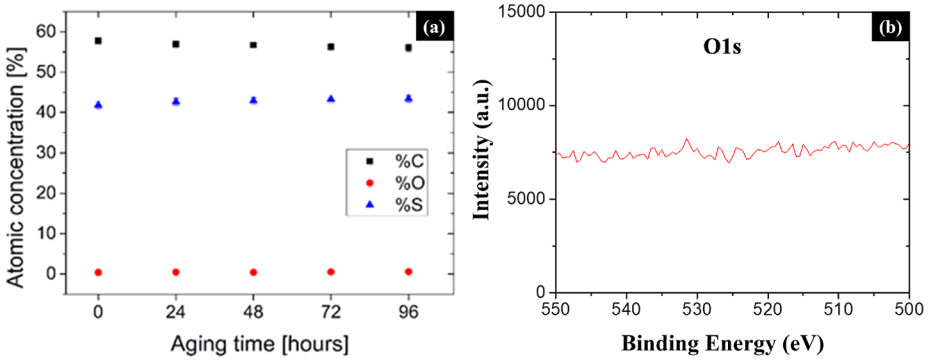


**Figure 5.** (a) Evolution of the atomic concentration of C, S, and O as a function of the PPF aging time. (b) High-resolution XPS spectra for 1s oxygen of the 96 h-aged PPF.

phenomenon is particularly prone to occur in our case as the PPF employed in this study exhibits increased chain mobility, as evidenced by its viscous state compared to conventional PPFs. In this context, ToF-SIMS measurements were conducted on PPFs at different aging times to evaluate the veracity of this hypothesis.

Given the abundance of peaks in ToF-SIMS spectra, a statistical treatment using the PCA method was employed for data analysis, a strategy recently developed in the context of plasma polymers to extract essential information regarding PPF surface chemistry.[35,36] The "score" plot from the PCA treatment of the ToF-SIMS spectra is depicted in Figure 4.

The dissimilarity between ToF-SIMS spectra (obtained from the several aging duration conditions) in Figure 4 correlates with the distance between points representing ToF-SIMS spectra positioned in the plot according to the surface fragmentation pattern of PPFs. The principal components (PC1 and PC2) axes capture 71.7% of the variance, with PC1 contributing 60.2% and PC2 11.5%. Consequently, only PC1 is employed for data interpretation. As shown in Figure 4, concerning the aging duration, the samples are well discriminated along the PC1 axis except those for 24 and 48 h of aging. Table 1 summarizes the most statistically significant peaks (i.e., peaks having a statistical weight > 90%) in the PC1 model, which are responsible for sample discrimination in the score plot. A positive or negative loading coefficient (giving the statistical weight) is associated with each $m/z$ signal. The higher the loading coefficient's absolute value, the higher the intensity variation of the corresponding peak from sample to sample. Positive loadings characterize the as-deposited PPF and the 24, 48, and 72 h-aged ones as they are positioned in the positive part of the score plot when considering the PC1 axis, while the reverse situation prevails for the 96 h-aged PPF. Insights from Table 1 also indicate that positive loadings predominantly correspond to sulfur-based fragments, while negative loadings are exclusively associated with hydrocarbonated fragments. This point will be discussed later. The "average fragment" chemical composition was evaluated for each loading category to evaluate the evolution of the cross-linking degree upon aging.[35] A $CH_2$ group of identical valence


https://doi.org/10.1021/acs.langmuir.4c01552
Langmuir XXXX, XXX, XXX−XXX

states replaced sulfur atoms in the considered fragments of the loadings. Carbon and hydrogen atoms were then tallied for each loading category and divided by the number of considered loadings. The calculated average fragments were $C_{5.4}H_{9.4}^+$ and $C_{4.7}H_{6.9}^+$ for negative and positive loadings, respectively. Beyond the average fragment, attention was directed to the C/H ratio, reflecting the cross-linking degree of each loading category. Notably, the C/H ratio remained relatively similar (0.57 vs 0.68) for both loading categories, indicating an almost equivalent cross-linking degree across samples. Furthermore, it is noteworthy that no oxygenated fragments were highlighted from PCA interpretation as critical peaks of the positive and negative loadings, suggesting stable oxygen content in the PPF over time.

The nearly constant values of the cross-linking degree of the PPF, whatever the aging duration, suggest a low concentration or the absence of trapped radicals in the plasma polymer network. Therefore, XPS measurements were carried out as a complement. Figure 5a depicts the evolution of the elemental chemical composition of the PPF over the aging time as deduced from XPS analysis. For the as-deposited PPF, the chemical composition is expected from our previous studies on the plasma polymerization of propanethiol.[37−39]

Interestingly, all atomic concentrations exhibit stability over time, underscoring the PPF's remarkable chemical durability (see Figure 5a). Furthermore, considering the detection limit of the XPS apparatus, no oxygen is identified in the spectra, as illustrated in Figure 5b for the 96 h-aged PPF. This behavior contrasts with the situation usually encountered for other PPFs, where a non-negligible uptake of oxygen takes place during the storage of the samples in the air.[40] The absence of postoxidation reactions over several days confirms our hypothesis about the absence of trapped radicals in the film, explaining the constant cross-linking degree with the aging duration. This unexpected behavior compared to other plasma polymer families might be tentatively explained by a reduced energy density brought by positive ions at the growing film interface at low substrate temperatures.[3]

Therefore, another mechanism is accountable for the increase in the viscosity of the layers. Returning to the PCA treatment of the ToF-SIMS spectra, the analysis of the loadings (Table 1) reveals a higher proportion of sulfur-based fragments over the aging duration. Considering the depth analysis of the ToF-SIMS equipment (i.e., 1 nm), this could indicate a preferential orientation of the sulfur-based functionalities toward the plasma polymer/air interface and signify structural alterations within the PPF as time progresses. Gengenbach et al. have demonstrated that irrespective of PPF oxidation, surface reorganization can occur in PPFs derived from different precursors over time.[24] Furthermore, intrinsic stress generated in the PPF matrix during growth is well-documented in the literature.[21,34,41] Based on these considerations, our hypothesis to elucidate the increase in viscosity with aging time involves a structural rearrangement in the PPF matrix. Considering the viscous nature of our PPF, chain mobility, compared to conventional solid PPFs, emerges as a predominant factor driving the effects of aging in PPFs. This enhanced mobility allows chain segments to adopt preferential positions, releasing intrinsic stress and minimizing the system's free energy through low-energy interactions (e.g., van der Waals forces) between closely positioned chain segments, resulting in network densification. Support for this explanation is found in the high atomic sulfur content in the PPF (~42%), as sulfur possesses high polarizability, enhancing the van der Waals interaction. This, in turn, reduces the mobility of the molecular segments, increasing the polymeric network's viscosity.

## 4. CONCLUSIONS

This study delves into the impact of the aging effect of liquid propanethiol plasma polymer on the dimensions of wrinkles in Al/PPF bilayers. The observed reduction in wrinkle dimensions is associated with changes in the mechanical properties of PPFs over time, specifically a decrease in the viscosity. Intriguingly, this transformation is not linked to alterations in the cross-linking degree as evidenced by ToF-SIMS measurements but rather to a network densification driven by the inherent chain mobility of the plasma polymer network. The XPS measurements corroborate these findings, emphasizing the absence of free radicals and a high sulfur content within the PPF. The absence of oxygen over time and the consistent chemical composition underline the unique aging mechanisms of the liquid sulfur-based PPF compared to other plasma polymer families. Notably, the aging duration of the PPF could also become an additional tuning factor for modulating the dimensions of the wrinkles in a wide range, giving more degrees of freedom for surface engineering. Our findings contribute to the fundamental understanding of PPF behavior and open avenues for the controlled design of nanostructured surfaces with enduring stability, holding significant potential for advancements in various technological applications such as flexible electronic devices,[9] superhydrophobic coatings,[42] filtration membranes,[43] and biomedical applications.[44]

## AUTHOR INFORMATION


### Corresponding Author

**Damien Thiry** − *Chimie des Interactions Plasma-Surface (ChIPS), Université de Mons, B-7000 Mons, Belgium;* orcid.org/0000-0001-6703-1512; Email: damien.thiry@umons.ac.be

### Authors

**Suyog A. Raut** − *Chimie des Interactions Plasma-Surface (ChIPS), Université de Mons, B-7000 Mons, Belgium*

**Nathan Vinx** − *Chimie des Interactions Plasma-Surface (ChIPS), Université de Mons, B-7000 Mons, Belgium*

**David Tromont** − *Chimie des Interactions Plasma-Surface (ChIPS), Université de Mons, B-7000 Mons, Belgium*

**Philippe Leclère** − *Laboratory for Physics of Nanomaterials and Energy (LPNE), Research Institute for Materials Science and Engineering, Université de Mons (UMONS), 7000 Mons, Belgium;* orcid.org/0000-0002-5490-0608

**Damien Cossement** − *Materia Nova Research Center, Parc Initialis, B-7000 Mons, Belgium*

**Rony Snyders** − *Chimie des Interactions Plasma-Surface (ChIPS), Université de Mons, B-7000 Mons, Belgium; Materia Nova Research Center, Parc Initialis, B-7000 Mons, Belgium*

Complete contact information is available at: https://pubs.acs.org/10.1021/acs.langmuir.4c01552


### Author Contributions

All authors have approved the final version of the manuscript. S.A. Raut: conceptualization, data curation, formal analysis, writing—original draft, and writing—review and editing. N. Vinx, D. Tromont, and D. Cossement: data curation and



https://doi.org/10.1021/acs.langmuir.4c01552
Langmuir XXXX, XXX, XXX−XXX

formal analysis. P. Leclère and R. Snyders: writing—review and editing. D. Thiry: supervision, conceptualization, formal analysis, funding acquisition, and writing—review and editing.

### Notes

The authors declare no competing financial interest.

## ■ ACKNOWLEDGMENTS

The work leading to this publication has received funding from the European Union's Horizon Europe research and innovation program under grant agreement no. 101092723/IBAIA. UK participants in Horizon Europe Project IBAIA are supported by UKRI grant no. 10062902 (MODUS). The FNRS partially supports the research at LPNE—FNRS grands 'Equipment's (40007941)—2022 Interuniversity Platform for the Analysis of the Nanoscale Properties of Emerging Materials and their Applications Ipanema grant.

## ■ ABBREVIATIONS

PPF, plasma polymer film; ToF-SIMS, time-of-flight secondary ion mass spectrometry; XPS, X-ray photoelectron spectroscopy; AFM, atomic force microscopy

## ■ REFERENCES

(1) Thiry, D.; Reniers, F.; Snyders, R. A Joint Mechanistic Description of Plasma Polymers Synthesized at Low and Atmospheric Pressure. *Surf. Modif. Polym.* **2019**, 67−106.

(2) Snyders, R.; Hegemann, D.; Thiry, D.; Zabeida, O.; Klemberg-Sapieha, J.; Martinu, L. Foundations of Plasma Enhanced Chemical Vapor Deposition of Functional Coatings. *Plasma Sources Sci. Technol.* **2023**, *32* (7), 074001.

(3) Vinx, N.; Leclère, P.; Poleunis, C.; Delcorte, A.; Mathieu, P.; Cossement, D.; Snyders, R.; Thiry, D. The Influence of the Substrate Temperature on the Growth Mechanism of Amine- and Thiol-Based Plasma Polymers: A Comparative Study. *Plasma Processes Polym.* **2024**, *21* (3), 2300138.

(4) Biederman, H. *Plasma Polymer Films*; Imperial College Press, 2004.

(5) Bitar, R.; Cools, P.; De Geyter, N.; Morent, R. Acrylic Acid Plasma Polymerization for Biomedical Use. *Appl. Surf. Sci.* **2018**, *448*, 168−185.

(6) Asadian, M.; Onyshchenko, I.; Thiry, D.; Cools, P.; Declercq, H.; Snyders, R.; Morent, R.; De Geyter, N. Thiolation of Polycaprolactone (PCL) Nanofibers by Inductively Coupled Plasma (ICP) Polymerization: Physical, Chemical and Biological Properties. *Appl. Surf. Sci.* **2019**, *479*, 942−952.

(7) Liang, H.; Panepinto, A.; Prince, L.; Olivier, M.; Cossement, D.; Bousser, E.; Geng, X.; Li, W.; Chen, M.; Snyders, R.; Thiry, D. Study of the Synthesis of C:H Coating by PECVD for Protecting Mg-Based Nano-Objects. *Plasma Processes Polym.* **2020**, *17* (11), 2000083.

(8) Grundmeier, G.; Thiemann, P.; Carpentier, J.; Barranco, V. Tailored Thin Plasma Polymers for the Corrosion Protection of Metals. *Surf. Coat. Technol.* **2003**, *174*−*175*, 996−1001.

(9) Jacob, M. V.; Olsen, N. S.; Anderson, L. J.; Bazaka, K.; Shanks, R. A. Plasma polymerised thin films for flexible electronic applications. *Thin Solid Films* **2013**, *546*, 167−170.

(10) Thiry, D.; Vinx, N.; Damman, P.; Aparicio, F. J.; Tessier, P. Y.; Moerman, D.; Leclère, P.; Godfroid, T.; Desprez, S.; Snyders, R. The Wrinkling Concept Applied to Plasma-Deposited Polymer-like Thin Films: A Promising Method for the Fabrication of Flexible Electrodes. *Plasma Processes Polym.* **2020**, *17* (9), 2000119.

(11) Jung, J.-S.; Myung, S.-W.; Choi, H. S. Surface Modification of Polypropylene by Nitrogen-Containing Plasma. *Korean J. Chem. Eng.* **2008**, *25* (5), 1190−1194.

(12) Hegemann, D.; Indutnyi, I.; Zajíčková, L.; Makhneva, E.; Farka, Z.; Ushenin, Y.; Vandenbossche, M. Stable, Nanometer-Thick Oxygen-Containing Plasma Polymer Films Suited for Enhanced Biosensing. *Plasma Processes Polym.* **2018**, *15* (11), 1800090.

(13) Turri, R.; Davanzo, C. U.; Schreiner, W.; Da Silva, J. H. D.; Appolinario, M. B.; Durrant, S. F. Structural and Optical Properties of Chlorinated Plasma Polymers. *Thin Solid Films* **2011**, *520*, 1442−1445.

(14) Thiry, D.; Vinx, N.; Aparicio, F. J.; Moerman, D.; Lazzaroni, R.; Cossement, D.; Snyders, R. An Innovative Approach for Micro/Nano Structuring Plasma Polymer Films. *Thin Solid Films* **2019**, *672*, 26−32.

(15) Saboohi, S.; Coad, B. R.; Short, R. D.; Michelmore, A.; Griesser, H. J. Rational Approaches for Optimizing Chemical Functionality of Plasma Polymers: A Case Study with Ethyl Trimethylacetate. *Plasma Processes Polym.* **2021**, *18* (3), 2000195.

(16) Saboohi, S.; Short, R. D.; Coad, B. R.; Griesser, H. J.; Michelmore, A. The Physics of Plasma Ion Chemistry: A Case Study of Plasma Polymerization of Ethyl Acetate. *J. Phys. Chem. Lett.* **2019**, *10* (23), 7306−7310.

(17) Khelifa, F.; Ershov, S.; Habibi, Y.; Snyders, R.; Dubois, P. Free-Radical-Induced Grafting from Plasma Polymer Surfaces. *Chem. Rev.* **2016**, *116*, 3975−4005.

(18) Vandenbossche, M.; Hegemann, D. Recent Approaches to Reduce Aging Phenomena in Oxygen- and Nitrogen-Containing Plasma Polymer Films: An Overview. *Curr. Opin. Solid State Mater. Sci.* **2018**, *22*, 26−38.

(19) Thiry, D.; Pouyanne, M.; Cossement, D.; Hemberg, A.; Snyders, R. Surface Engineering of Bromine-Based Plasma Polymer Films: A Step toward High Thiol Density Containing Organic Coatings. *Langmuir* **2018**, *34* (26), 7655−7662.

(20) Coad, B. R.; Favia, P.; Vasilev, K.; Griesser, H. J. Plasma Polymerization for Biomedical Applications: A Review. *Plasma Processes Polym.* **2022**, *19*, 2200121.

(21) Vinx, N.; Damman, P.; Leclère, P.; Bresson, B.; Fretigny, C.; Poleunis, C.; Delcorte, A.; Cossement, D.; Snyders, R.; Thiry, D. Investigating the Relationship between the Mechanical Properties of Plasma Polymer-like Thin Films and Their Glass Transition Temperature. *Soft Matter* **2021**, *17* (44), 10032−10041.

(22) Vinx, N.; Tromont, D.; Chauvin, A.; Leclère, P.; Snyders, R.; Thiry, D. Designing Nanostructured Organic-Based Material by Combining Plasma Polymerization and the Wrinkling Approach. *Langmuir* **2023**, *39* (43), 15231−15237.

(23) Vandeparre, H.; Gabriele, S.; Brau, F.; Gay, C.; Parker, K. K.; Damman, P. Hierarchical Wrinkling Patterns. *Soft Matter* **2010**, *6* (22), 5751−5756.

(24) Gengenbach, T. R.; Vasic, Z. R.; Li, S.; Chatelier, R. C.; Griesser, H. J. Contributions of Restructuring and Oxidation to the Aging of the Surface of Plasma Polymers Containing Heteroatoms. *Plasmas Polym.* **1997**, *2* (2), 91−114.

(25) Vasilev, K.; Britcher, L.; Casanal, A.; Griesser, H. J. Solvent-Induced Porosity in Ultrathin Amine Plasma Polymer Coatings. *J. Phys. Chem. B* **2008**, *112* (35), 10915−10921.

(26) Thiry, D.; Britun, N.; Konstantinidis, S.; Dauchot, J. P.; Guillaume, M.; Cornil, J.; Snyders, R. Experimental and Theoretical Study of the Effect of the Inductive-to-Capacitive Transition in Propanethiol Plasma Polymer Chemistry. *J. Phys. Chem. C* **2013**, *117* (19), 9843−9851.

(27) Salez, T.; McGraw, J. D.; Cormier, S. L.; Bäumchen, O.; Dalnoki-Veress, K.; Raphaël, E. Numerical Solutions of Thin-Film Equations for Polymer Flows. *Eur. Phys. J. E* **2012**, *35* (11), 114.

(28) Eriksson, L.; Johansson, E.; Kettaneh-Wold, N.; Trygg, J. *Multi- and Megavariate Data Analysis: Part II: Advanced Applications and Method Extensions*; Umetrics Inc: Umea, Sweden, 2006.

(29) Chan, E. P.; Lin, Q.; Stafford, C. M. Quantifying the Elasticity and Viscosity of Geometrically Confined Polymer Films via Thermal Wrinkling. *J. Polym. Sci., Part B: Polym. Phys.* **2012**, *50* (22), 1556−1561.

(30) Xie, J.; Han, X.; Zong, C.; Ji, H.; Lu, C. Large-Area Patterning of Polyaniline Film Based on in Situ Self-Wrinkling and Its Reversible



https://doi.org/10.1021/acs.langmuir.4c01552
Langmuir XXXX, XXX, XXX−XXX

Doping/Dedoping Tunability. *Macromolecules* **2015**, *48* (3), 663−671.
(31) Bai, J.; Hu, K.; Zhang, L.; Shi, Z.; Zhang, W.; Yin, J.; Jiang, X. The Evolution of Self-Wrinkles in a Single-Layer Gradient Polymer Film Based on Viscoelasticity. *Macromolecules* **2022**, *55* (9), 3563−3572.
(32) Liu, A.; Yao, Y.; Yao, J.; Liu, T. Droplet Spreading Induced Wrinkling and Its Use for Measuring the Elastic Modulus of Polymeric Thin Films. *Macromolecules* **2022**, *55* (10), 3877−3885.
(33) Das, A.; Banerji, A.; Mukherjee, R. Programming Feature Size in the Thermal Wrinkling of Metal Polymer Bilayer by Modulating Substrate Viscoelasticity. *ACS Appl. Mater. Interfaces* **2017**, *9* (27), 23255−23262.
(34) Carneiro de Oliveira, J.; Airoudj, A.; Kunemann, P.; Bally-Le Gall, F.; Roucoules, V. Mechanical Properties of Plasma Polymer Films: A Review. *SN Appl. Sci.* **2021**, *3*, 656.
(35) Cossement, D.; Renaux, F.; Thiry, D.; Ligot, S.; Francq, R.; Snyders, R. Chemical and Microstructural Characterizations of Plasma Polymer Films by Time-of-Flight Secondary Ion Mass Spectrometry and Principal Component Analysis. *Appl. Surf. Sci.* **2015**, *355*, 842−848.
(36) Ligot, S.; Bousser, E.; Cossement, D.; Klemberg-Sapieha, J.; Viville, P.; Dubois, P.; Snyders, R. Correlation between Mechanical Properties and Cross-Linking Degree of Ethyl Lactate Plasma Polymer Films. *Plasma Processes Polym.* **2015**, *12* (6), 508−518.
(37) Aparicio, F. J.; Thiry, D.; Laha, P.; Snyders, R. Wide Range Control of the Chemical Composition and Optical Properties of Propanethiol Plasma Polymer Films by Regulating the Deposition Temperature. *Plasma Processes Polym.* **2016**, *13* (8), 814−822.
(38) Choukourov, A.; Biederman, H.; Kholodkov, I.; Slavinska, D.; Trchova, M.; Hollander, A. Properties of Amine-Containing Coatings Prepared by Plasma Polymerization. *J. Appl. Polym. Sci.* **2004**, *92* (2), 979−990.
(39) Pleskunov, P.; Nikitin, D.; Tafiichuk, R.; Shelemin, A.; Hanuš, J.; Kousal, J.; Krtouš, Z.; Khalakhan, I.; Kúš, P.; Nasu, T.; Nagahama, T.; Funaki, C.; Sato, H.; Gawek, M.; Schoenhals, A.; Choukourov, A. Plasma Polymerization of Acrylic Acid for the Tunable Synthesis of Glassy and Carboxylated Nanoparticles. *J. Phys. Chem. B* **2020**, *124* (4), 668−678.
(40) Kasparek, E.; Thiry, D.; Tavares, J. R.; Wertheimer, M. R.; Snyders, R.; Girard-Lauriault, P. L. Growth Mechanisms of Sulfur-Rich Plasma Polymers: Binary Gas Mixtures versus Single Precursor. *Plasma Processes Polym.* **2018**, *15* (7), 1800036.
(41) Abadias, G.; Chason, E.; Keckes, J.; Sebastiani, M.; Thompson, G.; Barthel, E.; Doll, G.; Murray, C.; Stoessel, C.; Martinu, L. Review Article: Stress in thin films and coatings: Current status, challenges, and prospects. *J. Vac. Sci. Technol., A* **2018**, *36* (2), 020801.
(42) Hossain, M. M.; Trinh, Q. H.; Nguyen, D. B.; Sudhakaran, M. S. P.; Mok, Y. S. Formation of Plasma-Polymerized Superhydrophobic Coating Using an Atmospheric-Pressure Plasma Jet. *Thin Solid Films* **2019**, *675*, 34−42.
(43) Bally-Le Gall, F.; Mokhter, A.; Lakard, S.; Wolak, S.; Kunemann, P.; Fioux, P.; Airoudj, A.; El Yakhlifi, S.; Magnenet, C.; Lakard, B.; Roucoules, V. Poly(Allylamine) Plasma Polymer Coatings for an Efficient Retention of Ni(II) Ions by Ultrafiltration Membranes. *Plasma Processes Polym.* **2019**, *16* (3), 1800134.
(44) Macgregor, M.; Vasilev, K. Perspective on Plasma Polymers for Applied Biomaterials Nanoengineering and the Recent Rise of Oxazolines. *Materials* **2019**, *12* (1), 191.


https://doi.org/10.1021/acs.langmuir.4c01552
*Langmuir* XXXX, XXX, XXX−XXX